PROCEEDINGS, 48th Workshop on Geothermal Reservoir Engineering
Stanford University, Stanford, California, February 6-8, 2023
SGP-TR-224

A Review of Drilling, Completion, and Stimulation of a Horizontal Geothermal Well System in North-Central Nevada

Jack Norbeck, Timothy Latimer, Christian Gradl, Saurabh Agarwal, Sireesh Dadi, Eric Eddy, Steven Fercho, Camden Lang, Emma McConville, Aleksei Titov, Katharine Voller, and Mark Woitt

Fervo Energy, 114 Main Street, Suite 220, Houston, Texas 77002

jack@fervoenergy.com

Keywords: Horizontal drilling, hydraulic stimulation, proppant, nearfield EGS, fiber optic sensing.

ABSTRACT

In this paper, we present the drilling and completion results for Injection Well 34A-22 and Production Well 34-22, two horizontal geothermal wells that were drilled and completed successfully at the Blue Mountain field in northern Nevada. The wells were designed as an injection and production well pair to deliver flow rates of approximately 1250 gpm. The well paths targeted static reservoir temperatures between 350 °F to 400 °F, as required for commercial production at the Blue Mountain power plant facility.

The geologic setting at Blue Mountain is representative of many areas throughout the Basin and Range Province with high quality geothermal resource potential. The lateral sections of the wells targeted the Grass Valley formation, a Mesozoic metasedimentary formation comprised predominantly of interbedded phyllite and quartzite, as well as intrusive diorite and dikes and sills. The horizontal wells were placed in a southern reservoir compartment believed to have relatively few large-scale faults and low intrinsic permeability.

A major project highlight was the ability to successfully drill fully horizontal, large diameter hole sections along the curve and lateral sections of both wells. While building the curve from vertical to horizontal, we were able to achieve target build rates of 10 degrees per 100 ft. The production laterals were drilled with a 9 7/8" hole size to accommodate 7" production casing and permanent fiber optic cables.

Injection Well 34A-22 was stimulated with a 16-stage plug-and-perf hydraulic stimulation treatment with proppant. A total of approximately 267,000 bbl (11.2 million gal) of slickwater fluid and 7.3 million lbs of proppant were pumped during the stimulation treatment. The stimulated reservoir volume geometry was characterized using several independent reservoir diagnostics approaches, including microseismic monitoring, fiber optic strain sensing, pressure transient analysis, and offset well pressure monitoring. The dimensions of the stimulated reservoir volume were estimated to be roughly 1800 ft x 3000 ft x 750 ft, which is sufficient to meet the reservoir performance requirements of this project.

Both horizontal wells were drilled from the same pad. Optimal placement of the lateral on Production Well 34-22 required building a complex, three-dimensional curve with a significant amount of back-build and lateral step-out, representing a significant de-risking step for future projects where drilling multiple wells from a single pad may be required.

By completing this project successfully, we have demonstrated that currently no technical barriers exist to drilling horizontal wells and completing them with a multistage stimulation treatment approach in hard rock, high-temperature geothermal formations.

1. INTRODUCTION

Firm, zero-carbon, dispatchable resources are key to unlocking a fully decarbonized electricity sector (Sepulveda et al., 2018). Geothermal power can play that role, but in order to contribute a significant fraction of the energy mix geothermal projects must be deployed with speed and scale that the industry has not yet achieved (Ricks et al., 2022). Leveraging technology innovations from the unconventional oil and gas industry provides a pathway to unlocking new geologic resources and improving project economics in a way that could enable geothermal developers to mimic the rapid scale-up observed in shale development over the past two decades (Gradl, 2018; Latimer and Meier, 2017; Norbeck et al., 2018; Shiozawa and McClure, 2014).

Fervo Energy is developing a geothermal reservoir development strategy based on a well design that involves horizontal drilling and multistage hydraulic stimulation treatments. Fervo's horizontal well design results in geothermal systems where injection and production wells are connected in the subsurface by a set of hydraulically conductive fractures. These fractures act as flow pathways between the wells and provide sufficient contact area with the geothermal reservoir to enable sustained heat recovery over the life of the system.

Horizontal drilling has the potential to improve geothermal project economics significantly by providing greater access to the target reservoir volume, more consistent flow rates, more uniform flow distribution throughout the reservoir volume, and greater total heat transfer surface area. In addition, horizontal well designs offer many engineering design decisions that can be optimized to improve reservoir performance, including lateral length, offset well spacing, size of the stimulated reservoir volume, and fracture spacing along the wells. Horizontal well designs, stimulation treatment programs, and reservoir management strategies can be tailored for a given geologic resource which enables a broader range of geologies and locations to be developed than is possible with conventional geothermal development.

In field-scale development programs, horizontal drilling can result in a significant reduction in surface land use because multiple wells can be drilled from a single pad location. Drilling many wells from the same pad can enable cascading cost savings opportunities, such as minimizing in-field rig moves, reducing drilling risk by drilling closely spaced vertical well sections, co-locating surface facilities infrastructure, and minimizing pipeline costs.

Perhaps most importantly, the advantages of horizontal drilling described here make it possible to replicate the dramatic learning curve cost-reductions that have been observed in the unconventional oil and gas sector over the last two decades. Drilling many wells in a condensed area allows for geologic, technical and experience learning curves to be applied as a development project progresses, improving project economics over time (Latimer and Meier, 2017).

In this paper, we present the results from a commercial field-scale project that was designed to demonstrate the ability to drill, complete, and operate horizontal wells in high-temperature, hard rock geothermal formations. The project site is located in north-central Nevada adjacent to the Blue Mountain geothermal power facility (Fig. 1). Fervo designed and constructed a horizontal doublet system to produce approximately 5 MW of power.

Three wells were drilled successfully throughout 2022, including a deep vertical monitoring well and two horizontal wells that form an injection and production well pair. The target reservoir consists of metasediments (phyllite and quartzite) as well as granitic intrusives (diorite and granodiorite) with a maximum recorded temperature of approximately 375 °F at a depth of 8,000 ft. A multistage, multicluster hydraulic stimulation treatment with proppant was performed in July 2022. Data acquisition was a major focus of the project in order to characterize key reservoir performance metrics, including the size and geometry of the stimulated reservoir volume, the stimulation treatment effectiveness, and reservoir flow properties.

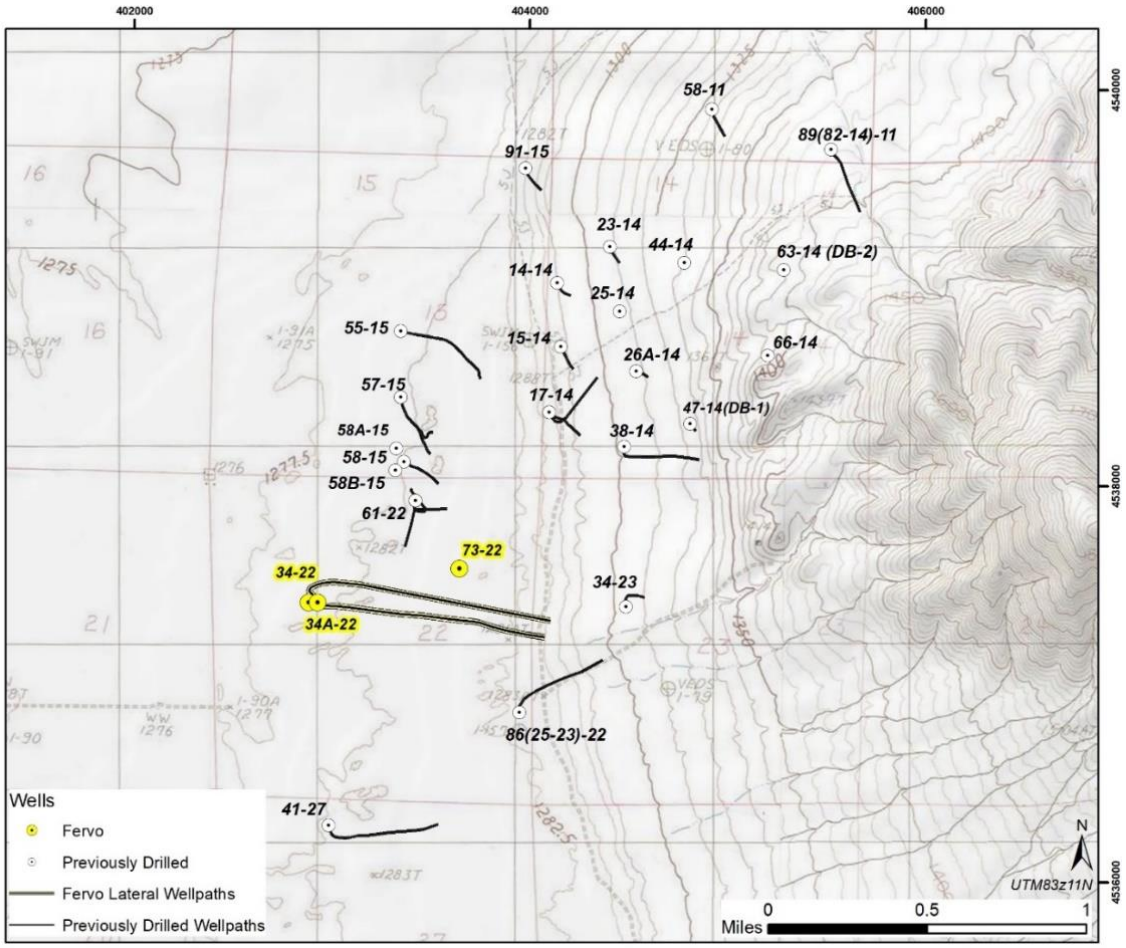

Figure 1: Map view of the Fervo Energy project site at the Blue Mountain Geothermal Field. Three new wells were drilled in 2022 (highlighted in yellow): Vertical Monitoring Well 73-22, Horizontal Injection Well 34A-22, and Horizontal Production Well 34-22. The horizontal wells were drilled to a true vertical depth of approximately 7,700 ft, and their productive lateral lengths are approximately 3,250 ft. Monitoring Well 73-22 is located roughly at the midpoint of the laterals and offset 700 ft to the north.

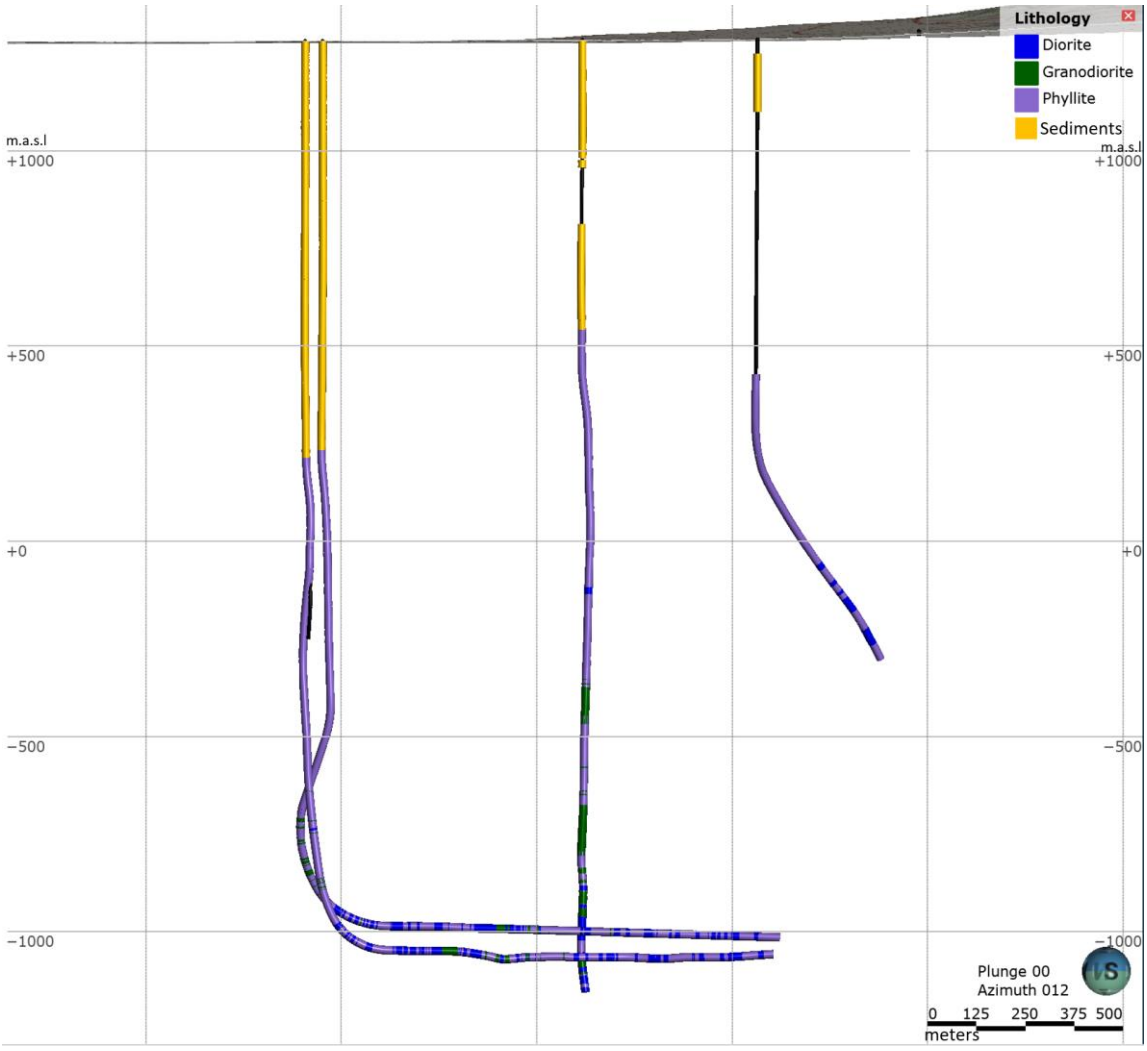

Figure 2: Cross-section view of the vertical and horizontal well trajectories.

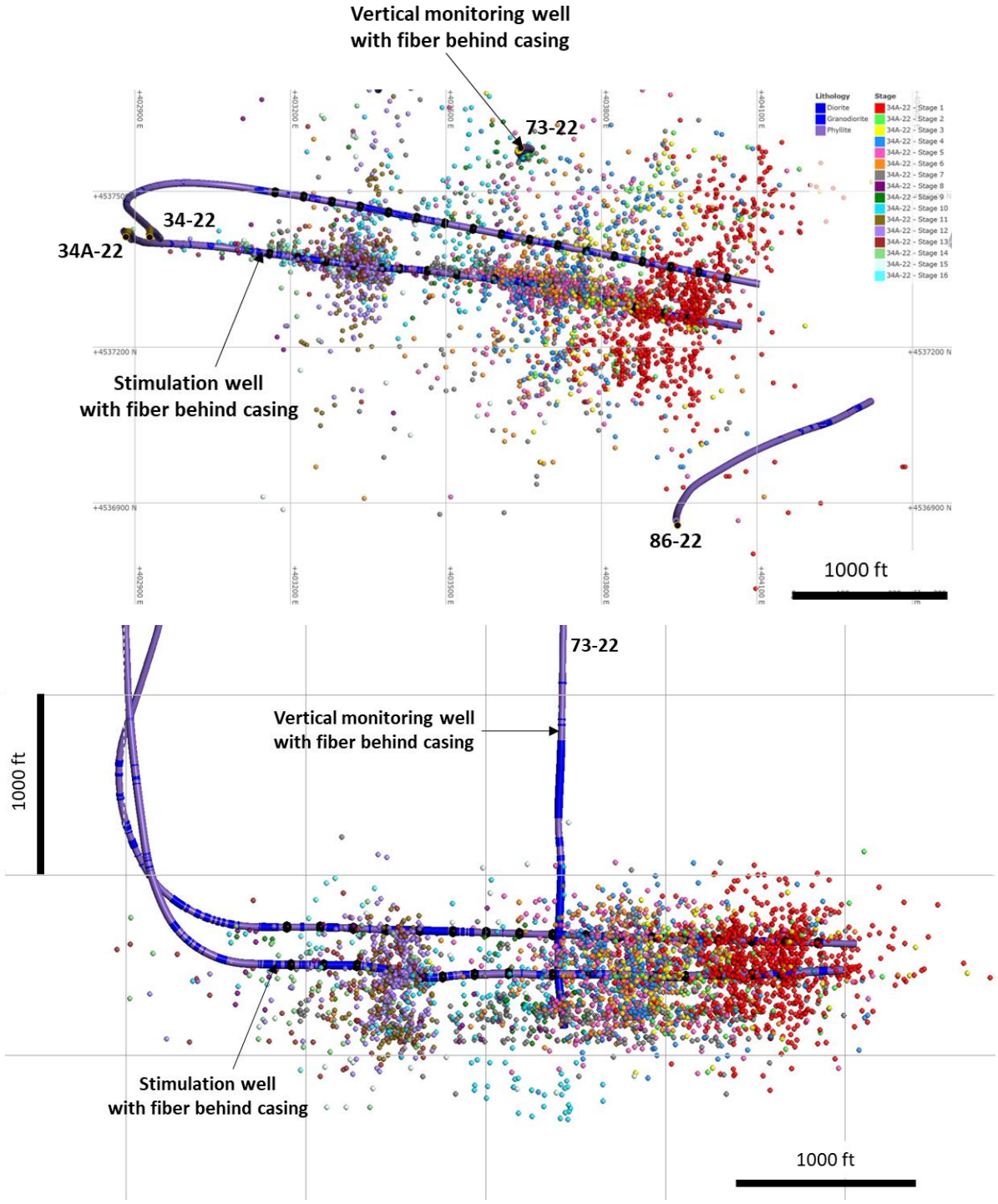

Figure 3: Map view of microseismic event locations detected with the fiber optic DAS array (top). Cross section view of the microseismic cloud (bottom). The colors of the dots are based on different stages and the color on the wells are showing the lithology identified based on cuttings, gamma ray, and other logs. The distribution of microseismic events were used to constrain the dimensions of the stimulated reservoir volume. Although the well path is shown here, note that Well 34-22 was drilled after the stimulation treatment occurred in Well 34A-22.

2. GEOLOGIC SETTING AND STATE OF STRESS

The overall stratigraphic framework at Blue Mountain consists of Miocene to present basin-fill deposits overlying Mesozoic phyllite. The phyllite is intruded by multiple phases of igneous dikes and sills interpreted to be Mesozoic and Tertiary in age. The range-front fault on the SW side of the Blue Mountain forms a prominent topographic break. On the NW side of Blue Mountain, silicified fault breccia is locally exposed in isolated outcrops surrounded by alluvium along the westernmost exposures of the surface trace of this fault. As previously noted by Szybinski (2005) and in later reports, the westernmost exposure of this fault zone is silicified, and the silicification was interpreted to be relict. Kinematic data collected from fault surfaces along the western half of the range-front fault indicate dextral-oblique motion.

Based on the map pattern of the faults and kinematic data, the Blue Mountain geothermal system is associated with a displacement transfer zone (e.g., Faulds and Hinz, 2015). In this structural model, the range-front along the SW side of the range is dextral-normal. This fault dies out into the basin west of the nose of the range and dextral shear is transferred to NE-striking normal faults that accommodate NW-SE extension in the form of pure dip-slip motion along the NW side of the Blue Mountain range. In this type of model, deep circulation would most likely be controlled by the N to NE-striking normal faults, near where they intersect the NW-striking dextral-normal fault system.

As is the case in most extensional settings, the wells located furthest out in the basin have the deepest depth to basement, especially 13-11 and 41-27 which are idle wells on the northern and southern margins of the field. The rest of the infield and nearfield wells show less variance in depth to basement as a function of distance to the range-front because faulting within the field is controlling the lithologic contacts. Stratigraphic control from the well data indicates that the basement progressively steps down to the NW, with the contact within each fault block gently dipping back towards the range front. The NW, N, and NE-striking faults which drop basement down in the core of the field are truncated to the south by the SW range front fault, which strikes SE to NW across the SW side of Blue Mountain and continues obscured under basin fill to the west. On the north end of the field, these faults merge into the NW range front of Blue Mountain.

South of the geothermal upflow and outflow zones of the primary hydrothermal system at Blue Mountain, there have been several wells drilled previously (86-22, 41-27, and 34-23) which exhibit relatively conductive temperature conditions and lack deep permeability or connectivity to the rest of the wellfield. This permeability boundary along the south side of the reservoir lies just south of Well 61-22 and has been interpreted to be associated with the down-dip projection of the southwest range-front fault (see Fig. 4). This recognized lack of deep permeability, reservoir connectivity, and elevated conductive temperatures radiating from the active system to the north makes the southern field (south of green line in Fig. 4) relatively compartmentalized, and therefore an ideal testbed for Fervo's horizontal well program.

Prior to Fervo's 2022 drilling campaign, there were four existing wells with image log data at Blue Mountain that were reviewed to gain insight of the local stress field (Fercho et al., 2023). From NE to SW, these wells had drilling-induced fractures (DIFs) that indicate an average SH_{max} azimuth of 010.3° (Well 58-11), 099.5° (Well 44-14), 021.4° (Well 26A-14), and 037.6° (Well 55-15). Image logs collected after Fervo drilled Monitoring Well 73-22 showed DIFs indicating an average SH_{max} orientation of 059.5° (northeast). The DIFs indicate a continued trend of clockwise rotation to the SW, although to a larger degree than was initially expected. As 73-22 is located approximately at the midpoint of Fervo's planned lateral wells, Fervo used this SH_{max} orientation to determine the optimal orientation of the planned lateral wells.

3. DRILLING AND WELL CONSTRUCTION ENGINEERING

The horizontal well designs were driven primarily by the following factors: a) the requirement of a 7" production casing string to enable commercial flow rates, b) the requirement of permanent fiber optic cable installation cemented behind the production casing for improved reservoir and wellbore diagnostics, c) a conservative casing program that would be robust against known and unknown geologic hazards in this first of a kind project, d) the local state of stress, and e) the three-dimensional temperature distribution in the reservoir.

The trajectory of Injection Well 34A-22 was planned and drilled as a "two-dimensional" well path. The trajectory of Production Well 34-22 was determined using a methodology that combined multiple datasets, including a three-dimensional geologic model, stress field data from image log interpretations, temperature distribution data, as well as information on the geometry of the stimulated reservoir volume, such as microseismic data and low-frequency distributed acoustic sensing data. Proppant was detected while drilling the 34-22 wellbore, confirming the well path intersected the stimulated reservoir volume.

3.1 Drilling Performance

The drilling sequence in the project was to first drill the vertical Monitoring Well 73-22, then drill Injection Well 34A-22, followed by drilling Production Well 34-22. Production Well 34-22 was drilled after the reservoir stimulation treatment was performed in Injection Well 34A-22, and the well path was planned to intersect the stimulated reservoir volume.

The days versus depth curves (DVD curves) for the three wells are shown in Fig. 5. Monitoring Well 73-22 was drilled to a total depth of 8,009 ft MD in 41 days. Injection Well 34A-22 was drilled to a total depth of 11,220 ft MD in 72 days. Production Well 34-22 was drilled to a total depth of 11,211 ft MD in 59 days. We were able to achieve significant improvements in drilling performance throughout the program, resulting in an 18% reduction in total drilling days between the first and second horizontal wells. The as-drilled well construction diagrams are shown in the Appendix in Figs. A1 – A3. Static temperature profiles were measured with the distributed temperature sensing (DTS) fiber optic cables and calibrated against the downhole temperature gauge in 73-22 as well as wireline temperature surveys. The equilibrated temperature profiles for the three wells are shown in Fig. 6. The maximum recorded downhole temperature was 376 °F.

Prior to the Fervo drilling campaign, at least 16 other deep geothermal wells had been drilled at the Blue Mountain field. In Fig. 7, we show a comparison of the DVD curves for all of the previously drilled wells and the three newly drilled Fervo wells. The Fervo wells were three out of the top five fastest wells drilled in the field, placing these wells in the top quartile in terms of drilling performance at Blue Mountain. The strong drilling performance relative to other wells in the same field is particularly notable given that these wells were drilled with significantly more complex well construction designs, including more casing strings, large hole diameters, build rates of up to 10° per 100 ft (where as the maximum build rate across the other Blue Mountain wells was 3° per 100 ft), and the horizontal drilling component. The Fervo wells were also three of the deepest wells drilled at Blue Mountain in terms of true vertical depth. While there is significant opportunity to continue to improve drilling performance of horizontal geothermal wells, the performance achieved in Fervo's three well drilling campaign at Blue Mountain – in which an 18% well-over-well reduction in drilling days was achieved – validates that no barriers exist to drilling horizontal wells today and demonstrates a clear cost reduction trajectory.

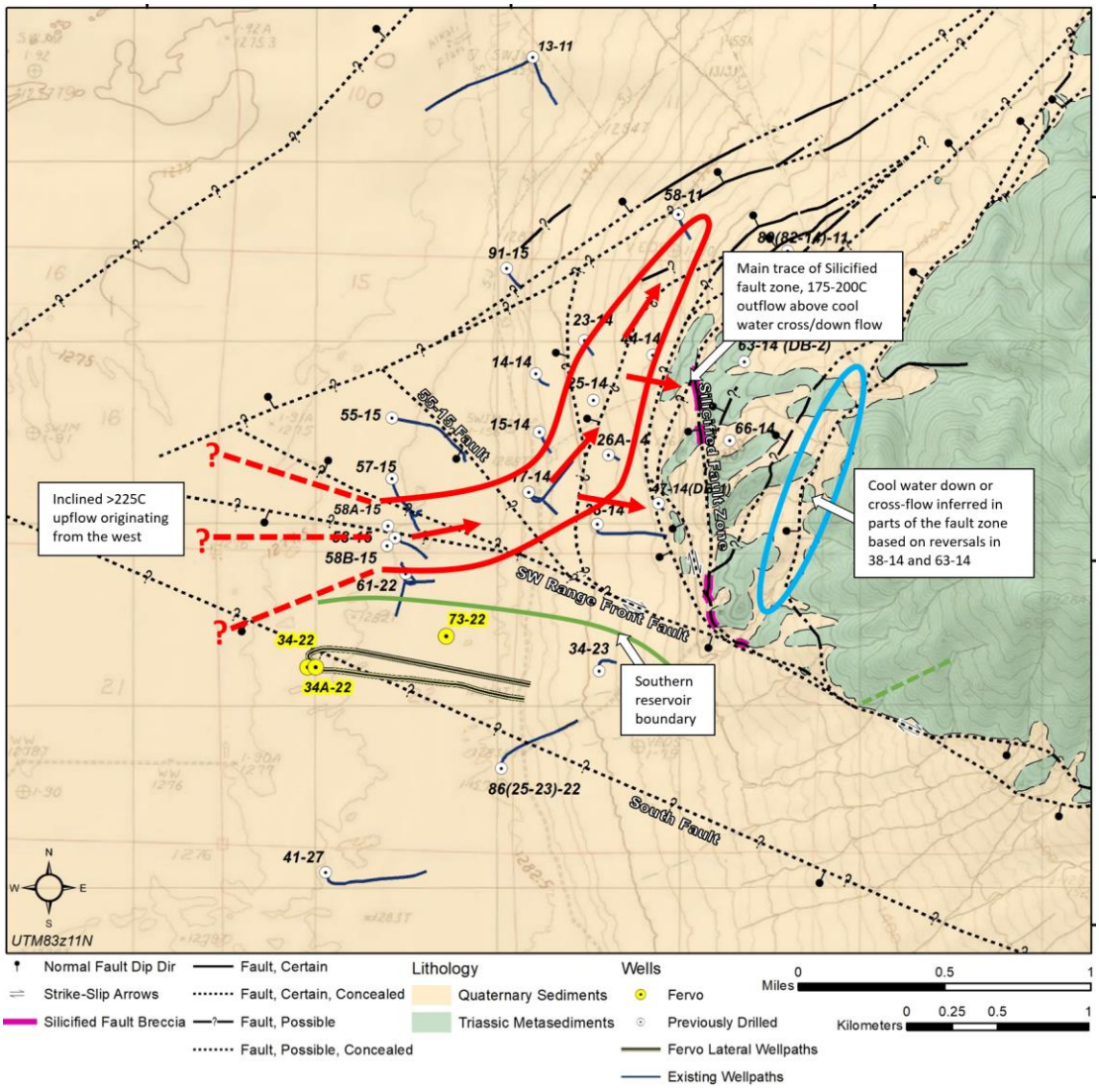

Figure 4: Fault and wellfield map showing the conceptual model, including an approximate southern boundary of the convective hydrothermal system.

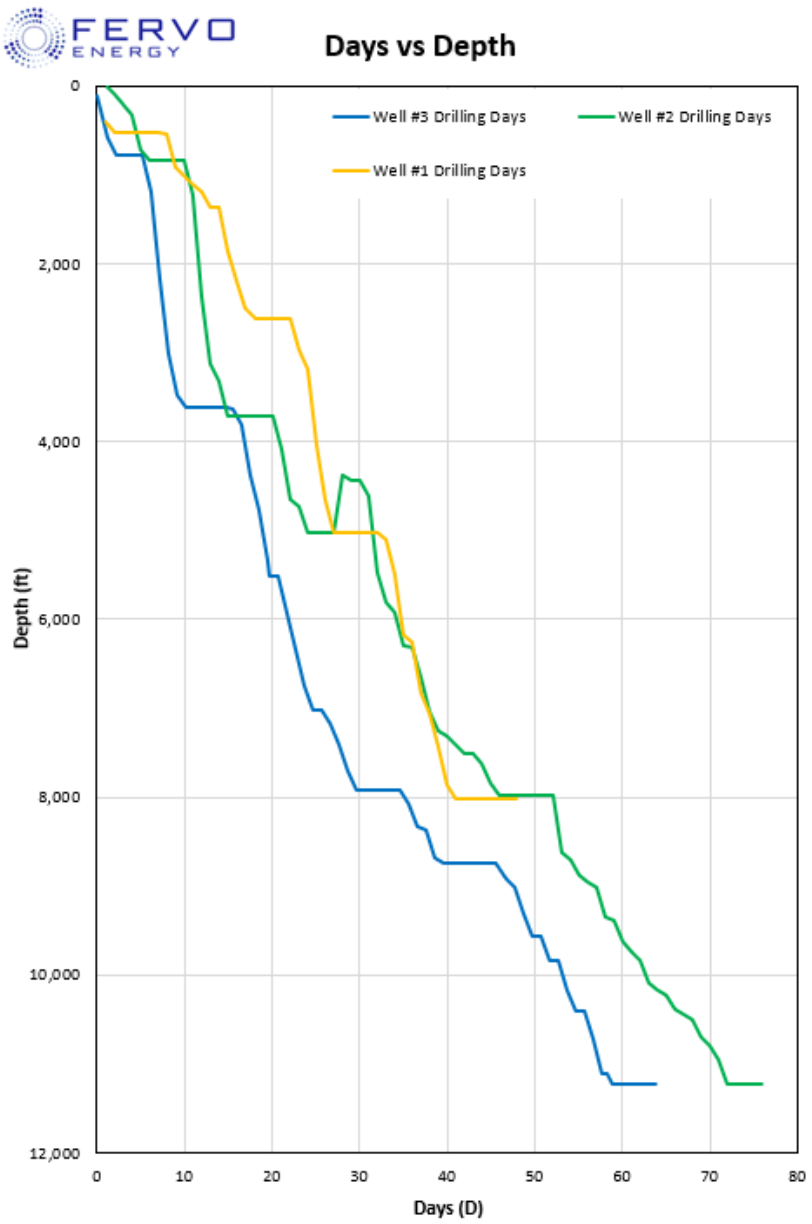

Figure 5: Days versus depth curves for Monitoring Well 73-22 (Well #1), Injection Well 34A-22 (Well #2), and Production Well 34-22 (Well #3). We achieved a significant reduction in drilling days (18%) from the first horizontal well to the second horizontal well.

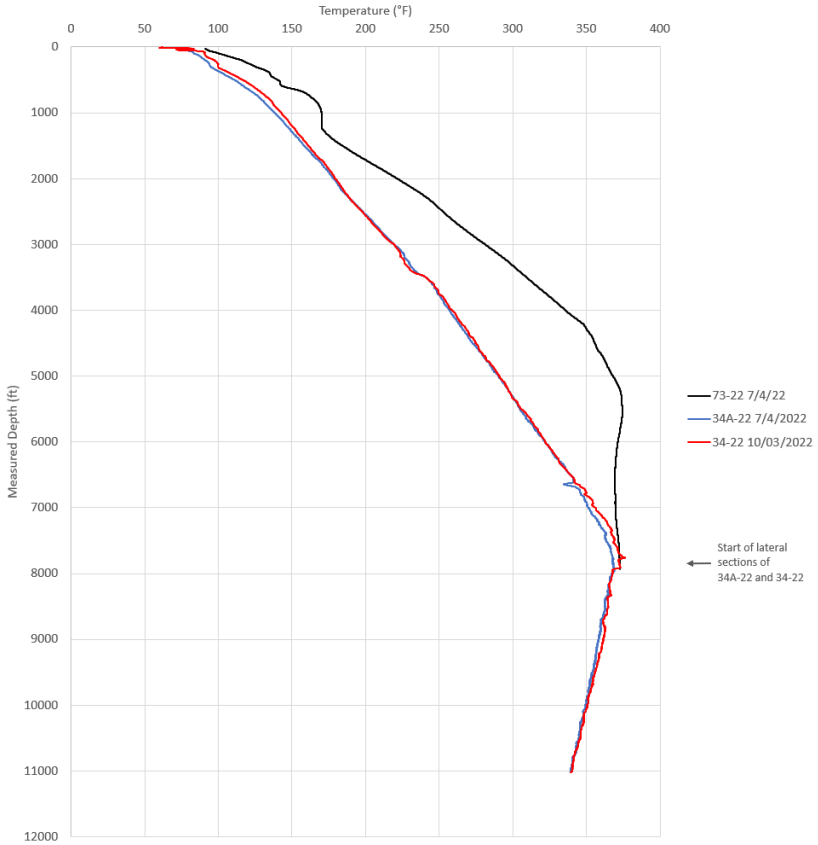

Figure 6: Equilibrated temperature profiles for Wells 73-22, 34A-22, and 34-22. The maximum recorded temperature on the three wells was 376 °F. Although the lateral sections on 34A-22 and 34-22 are at a constant true vertical depth, the temperature tends to decline slightly towards the toe due to the temperature distribution in the project area.

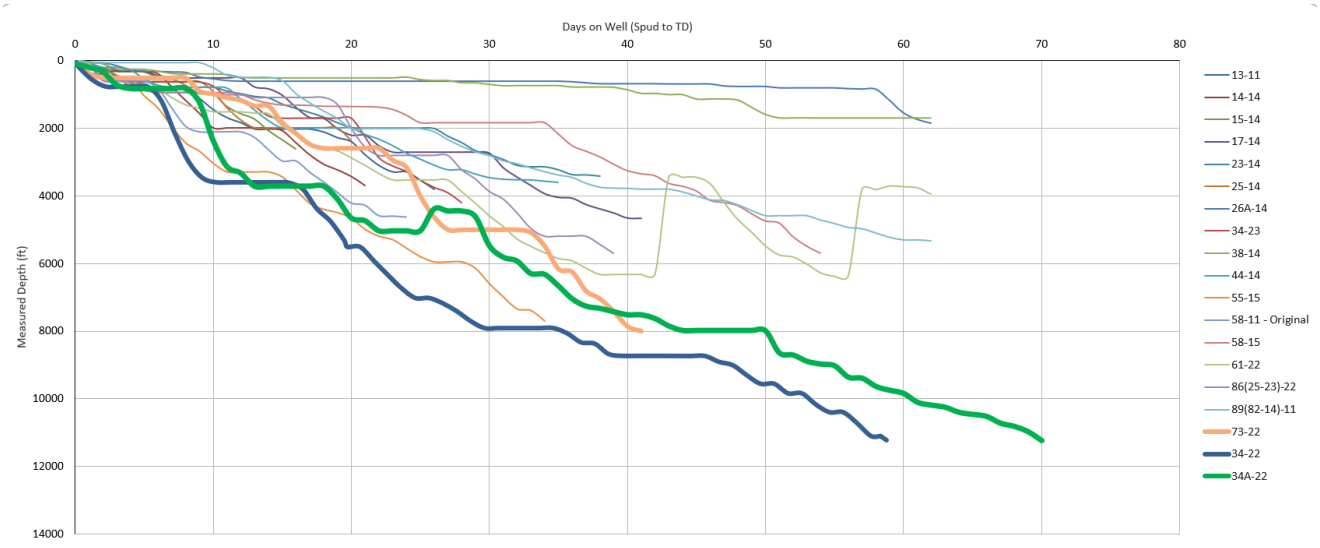

Figure 7: Days versus depth curves for all wells drilled at Blue Mountain field. Despite having significantly more complex well construction designs (more casing strings, larger hole diameters, larger build rates, and horizontal drilling), the three Fervo wells were in the top quartile of overall drilling speed.

3.2 Downhole Temperature Conditions During Drilling

A technical challenge cited commonly as a barrier to horizontal drilling in high-temperature formations is that the downhole temperature conditions that the bit, directional tools, mud motors (or rotary steerable systems) are too high for the tools to work effectively. In our project, we anticipated static reservoir temperatures exceeding 350 °F prior to drilling, and this was validated in the post-drill equilibrated temperature surveys (maximum recorded temperature was 376 °F). We recorded drilling fluid temperatures into and out of the mud pits as well as downhole temperatures with a MWD sensor located about 92 ft behind the drill bit. We observed that the bottomhole temperature remained significantly below the static formation temperature due to circulating the drilling fluid. The maximum temperature downhole temperature recorded while drilling the lateral was approximately 225 °F (see Fig. 8). The average circulation rate was approximately 800 gpm. We did not experience any MWD or directional tool failures related to temperature while drilling 34A-22 and 34-22. We do not consider downhole temperature to be a limiting factor for drilling performance for wells of similar depth and temperature as described here, however this may need to be considered further in cases where significant longer laterals are planned or if higher temperature formations are targeted.

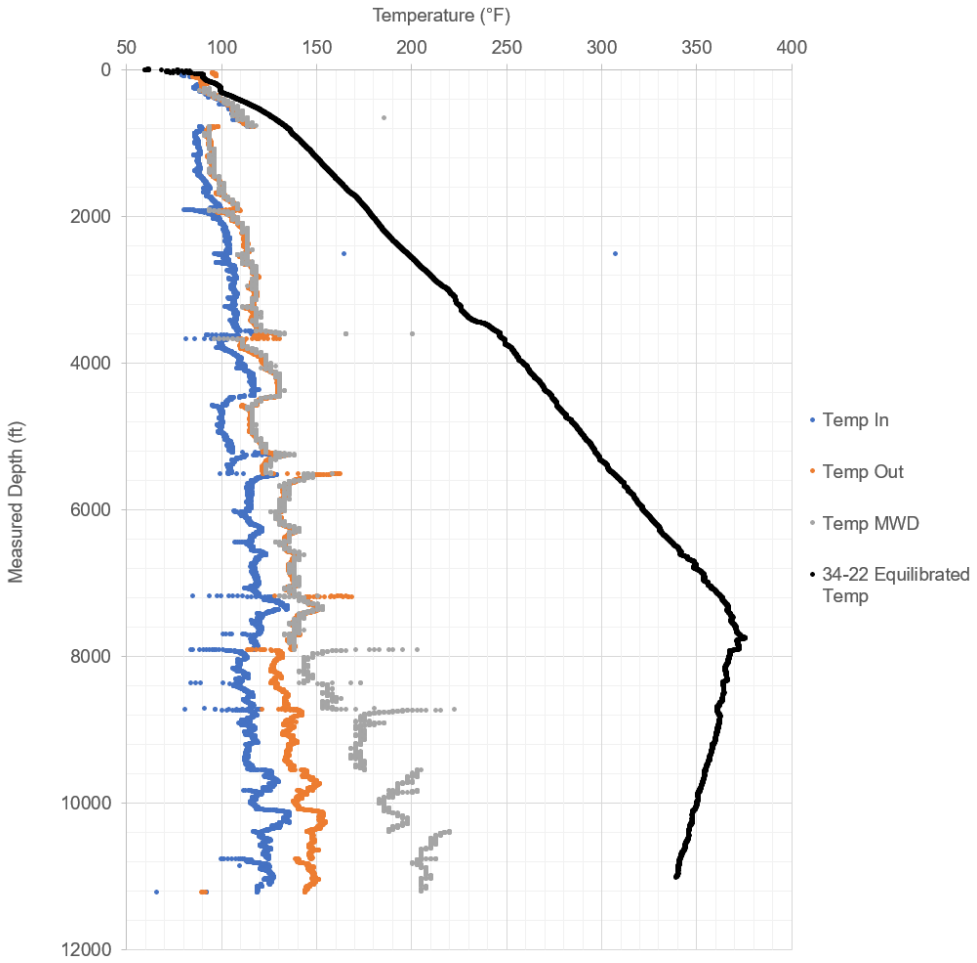

Figure 8: Drilling fluid temperatures measured while drilling Well 34-22. Inlet and outlet temperatures were measured at the mud pits, and the bottomhole temperature was measured using an MWD temperature sensor located approximately 92 ft behind the bit. For reference, the background equilibrated temperature profile is also shown. Despite the maximum equilibrated reservoir temperature of 376 °F, we observed that the downhole temperatures while drilling never exceeded 250 °F. Note that the average drilling fluid circulation rate was about 800 gpm.

4. COMPLETIONS ENGINEERING AND STIMULATION TREATMENT DESIGN

A 16-stage plug-and-perf hydraulic stimulation treatment was performed on Injection Well 34A-22 over a six-day period from July 21 – July 26, 2022. The plug-and-perf stimulation treatment method, which is now the most common stimulation method used in unconventional oil and gas wells, involves the following steps for a typical stage:

1. Rig up a wireline toolstring with a "flow-through" bridge plug and several perforation charges.
2. Lower the wireline toolstring into the well. The toolstring is conveyed by wireline until reaching the curve section of the well.
3. Pump trucks are engaged and the toolstring is pumped down the lateral by injecting into the well at rates of approximately 10 bpm until reaching the target location for the bridge plug.
4. The bridge plug setting tool is fired, and the plug is set a prespecified location along the lateral.
5. The wireline toolstring is pulled uphole until reaching the prespecified location for the deepest perforation cluster and the perforation charges are fired. This step is repeated for all perforation clusters in the given stage.
6. Wireline is pulled out of hole.
7. A ball is dropped in the wellhead and pumped downhole. A pressure spike on surface signals that the ball has seated in the bridge plug. The current stage is now isolated hydraulically from the previous stage.
8. The treatment is then pumped as designed, typically beginning with an acid spear of approximately 1000 gal of 15% HCl, followed by a pad of clean fluid, and then gradually increasing proppant concentration throughout the remainder of the stage. At the end of the stage, a sweep of clean fluid is pumped to flush the wellbore from any remaining proppant.
9. The pumps are shut down and the instantaneous shut-in pressure (ISIP) is recorded.

Each stage had roughly the same length of approximately 150 ft. All stages were planned with a similar perforation cluster design, with 6 clusters per stage and 6 perforation shots per cluster, except for Stages 12 and 13, which each had 9 clusters per stage and variable shots per cluster. The perforation clusters were designed with a limited entry style design (Gradl, 2018, Weiers et al., 2019), targeting approximately 1,500 psi of perforation friction.

The treatment design called for pumping a total of approximately 17,000 bbl of fluid and 540,000 lbs of proppant in each stage. The target injection rate was 100 bpm. The stimulation fluid was a slickwater treatment design with a low-concentration friction reducer additive. The proppant was a mixture of 100 mesh and 40/70 mesh silica sand, pumped at concentrations ranging from 0.25 to 1.5 ppg. Each stage lasted approximately 3 hours.

4.1 Evaluating Stimulation Treatment Effectiveness Using In-Well Fiber Optic Sensing Diagnostics

The treatment plot for a typical stage is shown in Fig. 9. The in-well fiber optics data enabled us to observe key downhole behavior in real-time before, during, and after each stage. This fiber optic data provides useful information on the stimulation treatment effectiveness and the downhole conditions that various tools are exposed to.

The in-well DAS data was used to verify whether fracture initiation occurred at each perforation cluster as well as the flow allocation across all clusters in the stage. In this example, we observed that all six perforation clusters broke down and received flow for the full duration of the stage. Taking the DAS amplitude signal as a proxy for flow rate at each perforation cluster, we observed that clusters 2, 3, and 5 were the most active, however all clusters accepted fluid and the overall flow uniformity index was calculated as 73% (the uniformity index ranged from 56% to 81% across all stages). The relatively low levels of acoustic activity downstream of the bridge plug indicate that good stage isolation was achieved.

During the stimulation treatment, the DTS data can be used to understand stage isolation and to determine if any leakage is occurring into the previous stage, either around the plug or behind the casing. In this example, some cooling was observed downstream of the plug in the first half of the stage, but toward the middle of the stage a clear warmback signal is observed. We attribute the relatively small amount of cooling early in the stage to most likely be caused by near-well fracture communication as fracture initiation occurred, as opposed to a leaky plug.

We were able to record in-well fiber optic sensing data for 13 out of the 16 stages. Upon analyzing the fiber data for all stages, we found that fracture breakdown and initiation occurred at 100% of the perforation clusters, regardless of the lithology that the perforation clusters were located in. In Fig. 10, we show a histogram of the estimated fluid volume attributed to each perforation cluster, and although there is some spread, we found that all clusters took flow during the stimulation treatment. The stages with 9 clusters also showed relatively good flow distribution, verifying that extreme limited entry completions (Somanchi et al., 2018; Weijers et al., 2019) are likely a viable path towards meaningful cost reductions in future drilling campaigns. In addition, we found no evidence of any bridge plug failures, indicating that the bridge plugs used in this project were rated to sufficient temperature and differential pressure ratings for the downhole conditions that were experienced.

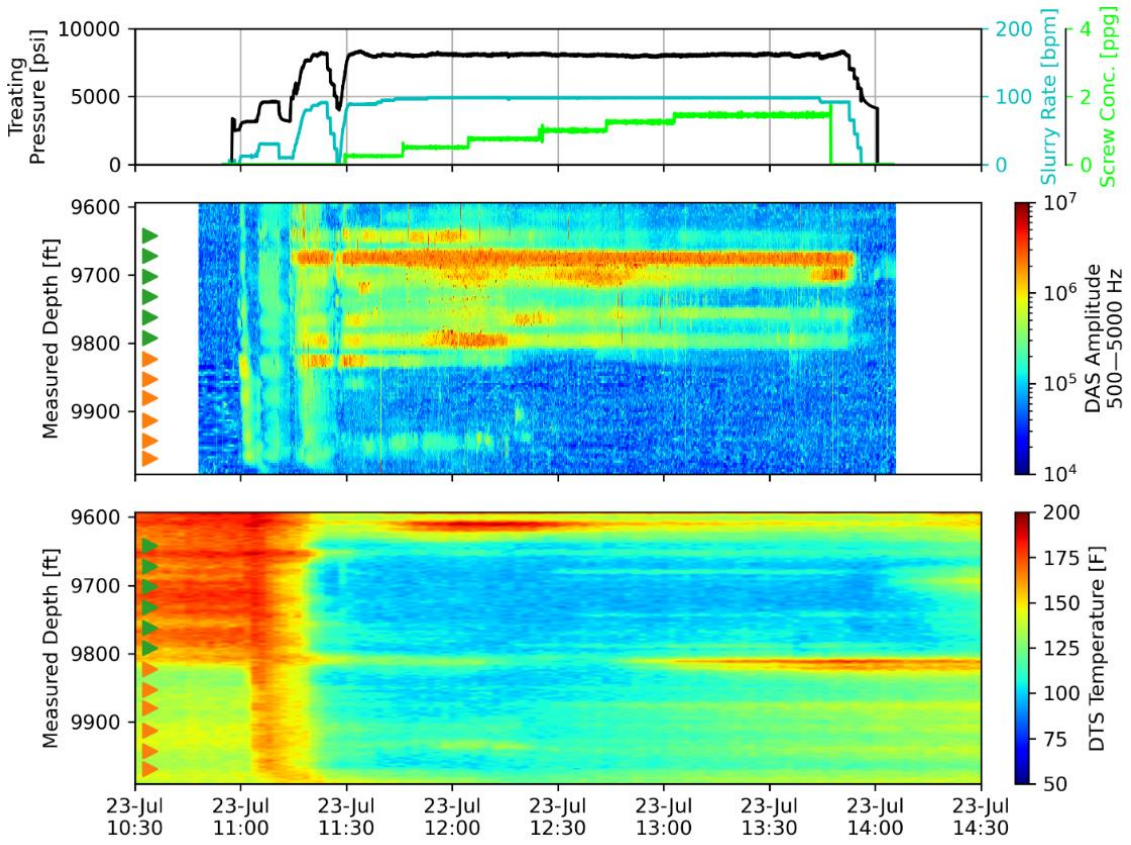

Figure 9: Treatment plot showing surface injection pressure, injection rate, and proppant concentration (top); DAS waterfall plot showing acoustic signal and location of the perforation clusters from the active stage and previous stage (middle); DTS waterfall plot showing the temperature variations along the well throughout the duration of the active stage (bottom).

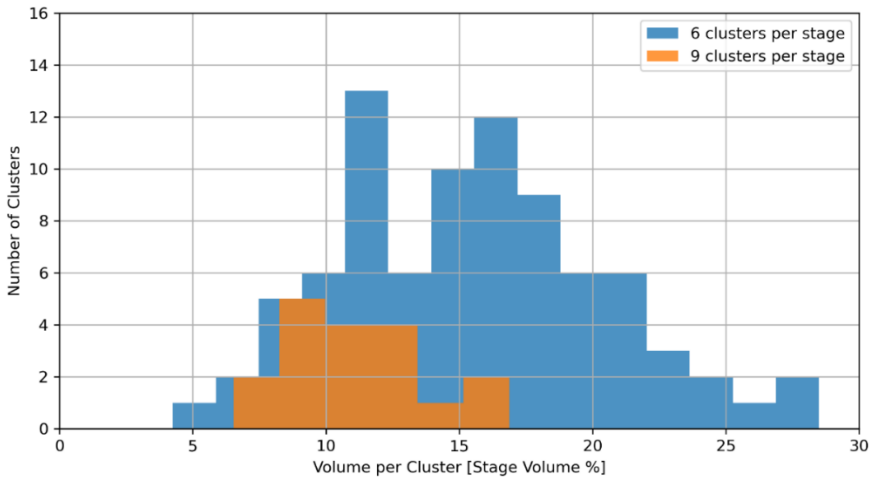

Figure 10: Histogram of the estimated total fluid volume allocated to each perforation cluster across the entire lateral. Fluid volumes and cluster allocation was estimated using the DAS acoustic intensity signal. The DAS data indicate that all clusters initiated and actively received flow during the stimulation treatment.

4.2 Downhole Temperature Conditions During Stimulation

Zonal isolation tool and technology development has been a focus area for the geothermal industry over the last several years. For multistage stimulation treatments in horizontal wells at geothermal conditions, there are several aspects of the operation that require careful attention. In this case, the tools must be capable of running in 7" 35# casing (ID = 6.004"). In addition, the maximum recorded bottomhole temperature was 374 °F. Based on conversations with vendors and other operators, to our knowledge, ball-drop flow-through bridge plugs had never been run in a horizontal well with a 7" production casing size or at these high temperature conditions.

We therefore performed a modeling study to characterize the anticipated downhole temperature conditions to inform our operational plans. We used a numerical reservoir simulator capable of modeling fluid flow, fracture propagation, and heat transfer with a fully coupled wellbore model that included wellbore heat transfer (McClure et al., 2022). We modeled a horizontal well scenario representative of Injection Well 34A-22. The formation temperature was 400 °F, fluid was injected at a rate of 100 bpm for 2 hours, and the injected fluid temperature was assumed to be 85 °F. We modeled two stimulation treatment stages near the toe of the lateral. The inter-stage duration between Stages 1 and 2 was 3 hours. In addition, we modeled a 12-hour warmback period to mimic a scenario where issues with the wireline assembly resulted in a long delay before pumping the next stage. Because we modeled the first two stages near the toe of the well and we assumed a relatively static formation temperature, this is taken to be a conservative scenario in terms of the warm back that could be expected. The relevant model properties are listed in Table 1.

In Fig. 11, we show the results of the numerical simulation. We observed that during injection while treating at a rate of 100 bpm, the wellbore temperature dropped to approximately 90 °F. Following shut-in, the wellbore warmed back rapidly within the first hour but then began to warm back more slowly. At the end of the first shut-in period, the wellbore had warmed back to a maximum temperature of about 265 °F. During the next stage, the wellbore again cooled down to about 90 °F. At the end of the 12-hour shut-in period, the wellbore had heated back up to approximately 300 °F. We therefore concluded that we should expect significant wellbore cooldown to occur during the field trial due to high-rate injection.

Table 1. Model properties used in the zonal isolation plug warmback analysis.

Property	Value
Static Formation Temp.	400 °F
Injection Fluid Temp.	85 °F
Treating Rate	100 bpm
Stage Duration	2 hours
Typical Inter-stage Duration	3 hours
Long Inter-stage Duration	12 hours

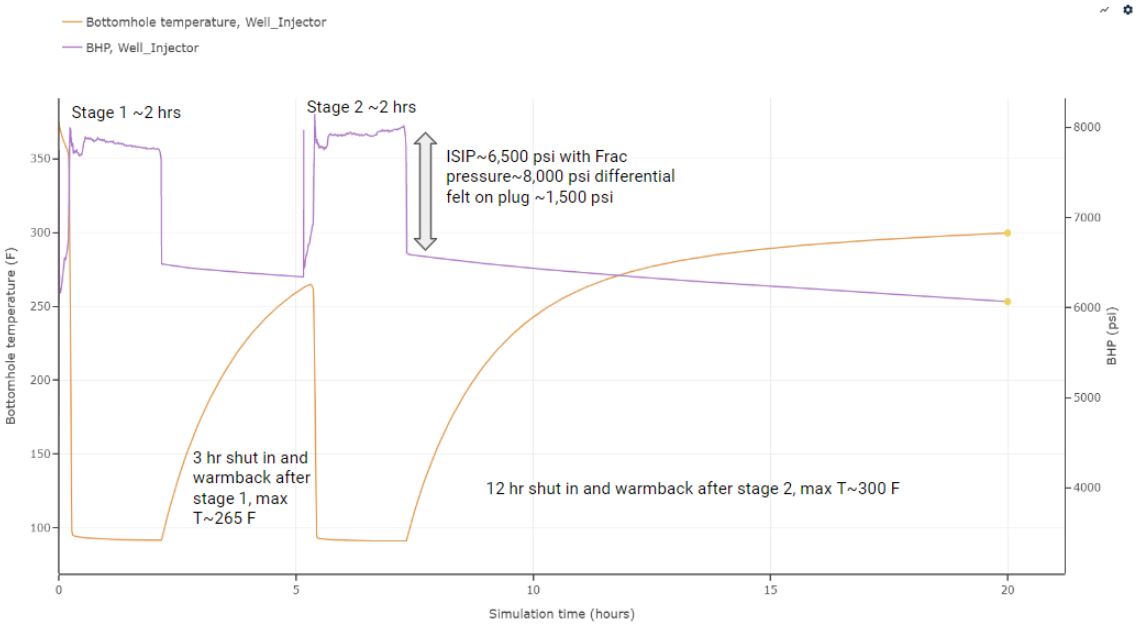

Figure 11: Simulation result showing bottomhole pressure and bottomhole temperature during a multistage stimulation treatment. Wellbore temperature cools down significantly while pumping at rates of 100 bpm, approaching the surface injection temperature. While the well is shut-in between stages, the well warms back up, but remains well below the static formation temperature. During a "worst-case" scenario with a long shut-in period, the wellbore temperature remains below 300 °F. These results were used to inform bridge plug selection for the stimulation treatment program.

We designed the stimulation field trial to include a test of three different zonal isolation bridge plug designs in order to better understand their performance. We identified two bridge plug designs that existed already on the market that could be run in 7" casing. These two plug designs were rated to downhole temperatures of 300 – 350 °F. In addition, Fervo collaborated with an industry partner to engineer, design, and fabricate a high-temperature ball-drop flow-through bridge plug that met our 7" casing requirements and was rated up to 450 °F. The technical specifications for the three types of plugs trialed in this project are shown in Table 2.

The composite plug (Plug A) was run in Stages 1 – 9. The aluminum plug (Plug B) was run on Stages 10 – 15. The high-temperature aluminum plug (Plug C) was run on Stage 16 (the final stage).

We were able to take advantage of the permanent fiber optic cable to record continuous DTS measurements that allowed us to monitor temperature along the lateral throughout the stimulation treatment. In general, we found no evidence for plug failure on any stage based on downhole fiber optic data or surface pressure responses.

To further understand the conditions that the plugs were actually exposed to, we analyzed the DTS measurements in greater detail. We expected to observe that the wellbore would experience significant cool down effects due to the high fluid injection rates during the treatment and during pump down activities.

In Fig. 12, we show the treatment plots and the DTS temperature trace at the Stage 16 plug location (MD = 8,181 ft) over the duration of Stages 15 and 16. The static formation temperature at this location was 370 °F based on the equilibrated temperature profile measured after drilling the well and prior to the stimulation treatment (see Fig. 6). By the end of Stage 15, the wellbore had cooled down to approximately 100 °F. In between stages, the wellbore warmed back, however, the maximum temperature observed prior to beginning pumping operations on Stage 16 was only 200 °F, significantly below the rated temperature of any of the plugs trialed in this project.

In Fig. 13, we show the temperature traces at the plug locations for several representative stages. We observed that the Stage 1 plug was subjected to the highest downhole temperature conditions, and all subsequent stages tended to be exposed to lower maximum temperatures. The Stage 1 plug experienced temperatures approaching 300 °F, having only been cooled down by relatively low-volume and low-rate injection while conveying the wireline assembly via pumpdown operations. However, even that minor amount of injection was sufficient to cool the wellbore below the temperature rating of Plug A, the lowest rated plug that was trialed. Subsequent stages are generally exposed to lower temperatures because of the remnant cooling effects of prior stages.

In this case, the modeling forecasts were able to predict the downhole temperature conditions during the stimulation treatment accurately. Based on real-time downhole measurements, we confirmed that bridge plugs do not need to be rated to the formation temperature because of the extreme cooling that occurs during wireline pumpdown and stimulation operations. In higher temperature formations, the rate of warmback in between stages will occur faster.

Table 2. Technical specifications for the three zonal isolation bridge plugs that were used in the field trial.

Plug Name	Fixture Material	Casing Size (in)	Casing Weight (lb/ft)	Max OD (in)	Pressure Rating (psi)	Temp. Rating (°F)
A	Composite	7	23 – 35	6.540	10,000	300
B	Aluminum	7	26 – 35	5.750	10,000	350
C	Aluminum	7	26 – 35	5.755	7,500	450

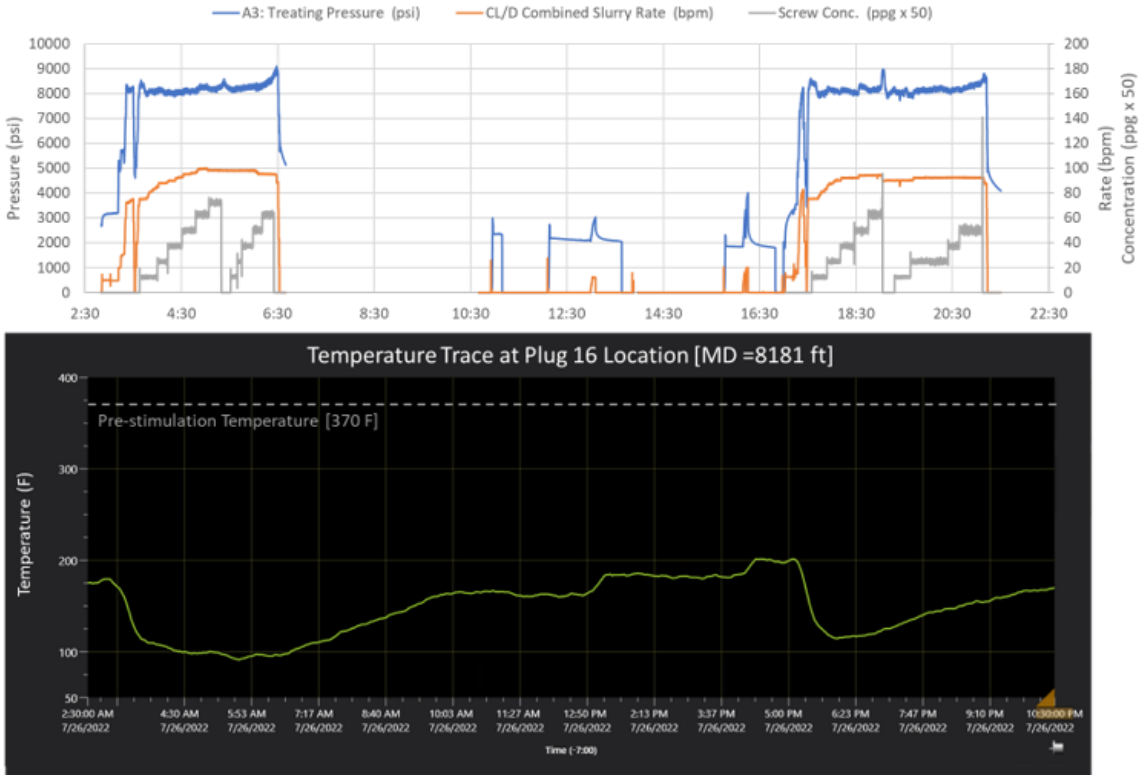

Figure 12: Treating plots (top) and DTS temperature trace at the Stage 16 plug location (bottom) recorded while treating Stages 15 and 16. The temperature that the bridge plug was exposed to never exceeded 200 °F, well below its rated temperature limit. The results of this field trial indicate that it is possible to rely on significant amounts of wellbore cooldown due to wireline pumpdown operations and high-rate injection during the stimulation treatment.

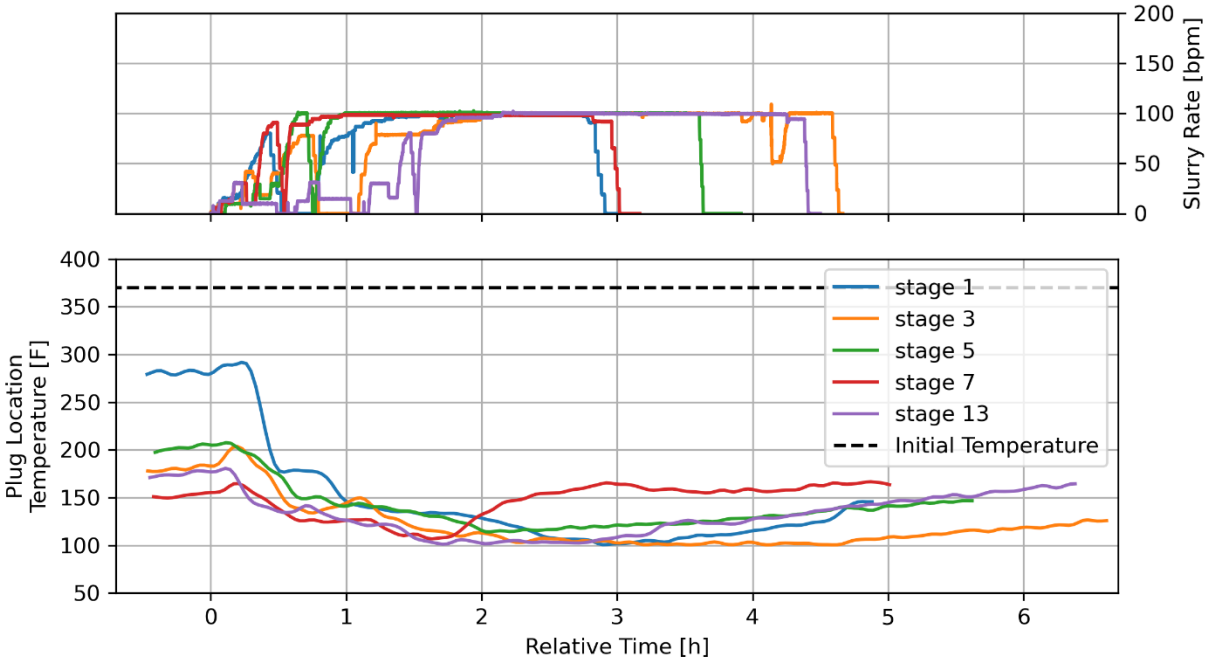

Figure 13. Typical treatment plots (top) and associated temperature traces at the plug locations (bottom) for several typical treatment stages. The plugs in the toe-most stages were exposed to the highest temperatures because they had not yet experienced as much cooldown. Later stages tended to be exposed to progressively lower temperature conditions.

5. STIMULATED RESERVIOR VOLUME DIAGNOSTICS

The purpose of the multistage, multicluster stimulation treatment program is to enhance the permeability of the reservoir, create extensive fracture surface area the enable sustainable heat transfer rates, and distribute flow uniformly throughout the reservoir to improve thermal recovery factors. The geometry of the stimulated reservoir volume (i.e., the length, height, orientation, and density of the fracture network created during the stimulation) is a useful metric for characterizing reservoir performance. Here, we describe how we use a variety of independent datasets to constrain the SRV geometry, including microseismic monitoring, strain monitoring using low-frequency distributed acoustic sensing fiber optics, and reservoir pressure monitoring using permanent bottomhole pressure gauges in offset wells.

We found that a reasonable estimate of the SRV size was approximately 1,800 ft x 750 ft x 3,000 ft. In a separate study, we evaluate the heat and place and power capacity of the horizontal doublet well system, and found that the system is capable of producing approximately 5 MW of electric power.

5.1 Microseismic Monitoring

The stimulation of Injection Well 34A-22 produced a significant number of microseismic events, which were detected with a favorable signal-to-noise ratio on multiple permanent fiber optic cables. A total of 5,200 events were observed on the vertical monitoring well. While the range of magnitudes varied from -2 to 1.5, the majority of events were below 0.5 and could be confidently detected on the fiber. A subset of the 5,200 events identified on the vertical fiber was also detected on the horizontal fiber, and the distribution of these events is shown in Fig. 3. The merged data from the vertical and horizontal fibers significantly improves the confidence of the event locations. However, the measurements of axial strain along the fibers imply that there is inherent uncertainty in the event location, particularly in the horizontal directions.

The azimuth of the individual stage events further confirms the stress orientation in the NE-SW direction identified from multiple sources across the Blue Mountain field. There appears to be a slight rotation of the microseismic (MS) cloud towards a more N-S orientation in the later stages near the heel. The event cloud extends approximately 1000 ft in the direction of SHmax, with more extension observed towards the NE compared to the SW. It is possible that the events extend symmetrically around the well, but events to the south are further away from the vertical well and hence are more attenuated. There is a symmetric distribution of the microseismic events in the vertical direction, with events extending approximately 300 ft above and below the stimulated well. The microseismic events can also be identified as stripes in the low-frequency strain rate data, and there is a good correlation between the height of the microseismic events and the extension observed (in red) in the low-frequency strain rate data, suggesting that the fractures are extending about 300-500 ft shallower than the treatment well. The lack of fiber below the horizontal well prevents similar conclusions from being reached deeper to the well, but the microseismic data indicates that the fractures did extend 300 ft deeper.

The results presented here demonstrate that fiber-based multi-well distributed acoustic sensing (DAS) microseismic for geothermal fields has been successfully realized as a proof-of-concept at Blue Mountain. Fiber based microseismic event locations can inform importance fracture geometry parameters like fracture orientations, fracture length and height, and the fracture propagation rate. The absence of reliable three-component borehole tools that can operate at temperatures above 400 °F further highlights the importance of fiber-optic-based microseismic measurements. However, the resolution and accuracy of the events would likely have been significantly improved with the aid of three-component borehole measurements.

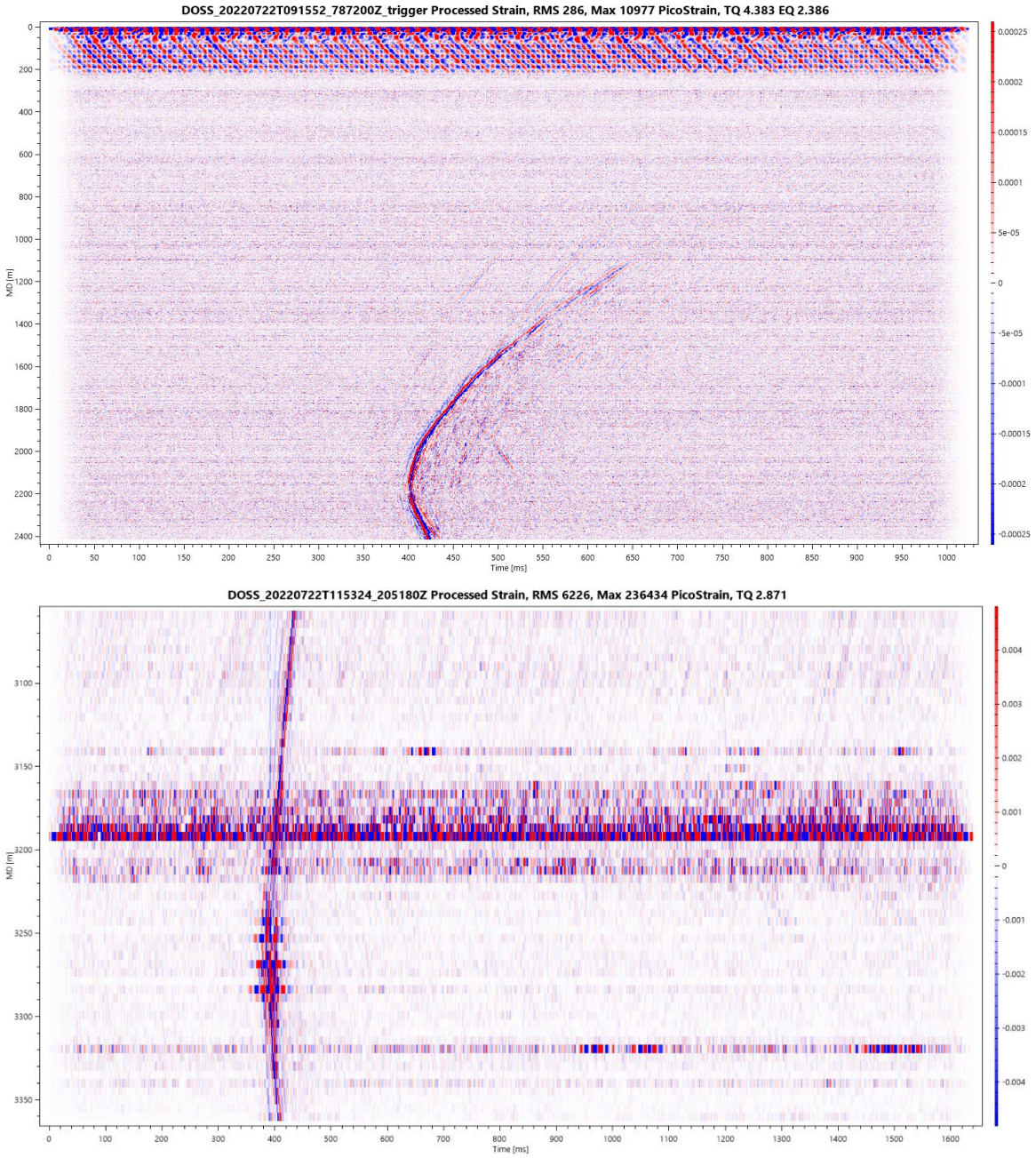

Figure 14: An example microseismic event identified on the vertical fiber (top). The apex of the S-wave can be used to infer the vertical depth of the microseismic event. The P-wave is a weak event further weakened at the peak due to the broad side sensitivity of the fiber. A converted S to P wave is detected for this event as evident at an approximate depth of 1500 m measured depth (MD). An example microseismic event detected by the horizontal fiber (bottom). The peak at 3260 m MD can be used to determine the location and distance of the event from the fiber in the azimuthal direction. The noise band from 3170-3190 m corresponds to the stimulation activity for the stage.

5.2 Strain Monitoring Using Low-Frequency DAS Fiber Optic Sensing

Distributed acoustic sensing records strain changes along the axial axis of a fiber cable in a wide range of frequencies from mHz to several kHz. The low-frequency part of the data (<0.05 Hz), or so-called LF-DAS, is commonly used during hydraulic stimulations to evaluate cross-well strain changes in offset horizontal wells (e.g., Jin and Roy, 2017) or vertical wells (e.g., Sherman et al., 2019) by interpreting the elastic stresses and strains that are induced by fracture propagation. In vertical monitoring wells, LF-DAS captures the change in the vertical component of the strain tensor. Figure 15 displays the recorded (middle) and modeled (bottom) cross-well strain change captured by the fiber cable installed in Monitoring Well 73-22. The recorded data are one of the first of their kind during the stimulation of a well in a geothermal formation. The model results exhibit similar features as observed in the field data and help to explain the observations.

We see this response because the process of fracture propagation causes a stress shadow effect away from the fracture, which is also coupled with a change in strain. The strength of this effect in a particular location is influenced by fracture aperture, fracture geometry, fracture azimuth, formation elastic properties, as well as the distance between the observation point relative to the propagating fractures. Generally, the closer the fracture plane is to the monitoring well, the stronger the observed response.

As the treatment of a given stage begins, we tend to observe extension of the fiber at depths between the upper and lower crack tips, and we observe compression above the upper crack tip (see model response shown in Fig. 16). The location of the polarity flip along the measured depth, observed in the LF-DAS data, is related to the fracture height. The polarity reversals in time are linked to fracture aperture changes associated with the treatment schedule. For the treatment stage shown in Fig. 16, the fracture plane was relatively close to the observation well (< 500 ft). In this case, the polarity flip location in depth can provide a reasonable estimate of fracture half-height. We see that the location of the polarity flips in depth is about 7,250 ft for recorded data and 7,300 ft for the model. The depth of the lateral at this stage is about 7,700 ft TVD. We can conclude that the fracture height was about 450 ft above the wellbore. The data indicate rapid fracture height growth. This height growth occurs rapidly, given that the polarity reversal in depth remains relatively constant throughout the treatment. Upon stage completion, we observe polarity reversal in time which is caused by a decrease in fracture aperture (note that the LF-DAS data is presented in units of strain rate and not total strain).

Figure 17 summarizes pressure and LF-DAS data recorded in the vertical monitoring offset well throughout the treatment of all 16 stages. In addition, the reservoir pressure response from the bottomhole pressure gauge at Monitoring Well 73-22 is shown in Fig. 17 (middle).

The first LF-DAS signal was observed during stage 1 stimulation of the 34A-22 well. It was someone unexpected to see this response, as fracture planes from the first stage are located more than 1,500 ft away from the 73-22 monitoring well. This observation is confirmed by modelling the LF-DAS data (Fig. 18) with a history-matched numerical reservoir model. The field and modeled data exhibit the same behavior. The shadow half-height indicated by the polarity flip is shortened from stage 1 to 9 and increased afterward. The amplitude of LF-DAS signals increased from Stage 1 to Stage 9 as the distance between stimulated fractures and the observation well reduced. The signal from Stage 9 has a complex behavior due to the very close (<100 ft) vicinity of multiple fracture planes to the monitoring fiber or even within the fracture corridor. This also indicates a fracture half-length of more than the horizontal offset between 34A-22 and 73-22 wells (about 800 ft). Stages 10 – 16 have weaker signals, which can be explained by fracture azimuth and possibly lower than 800 ft fracture half-length, which agrees with the model. Finally, we observed a regularly spaced signal from 6,000 ft to 6,500 ft around 26 July. The strain response in the fiber optic cable is very sensitive to temperature, and this signal is associated with heating (red) and cooling (blue) downhole instruments placed at this location for a short time.

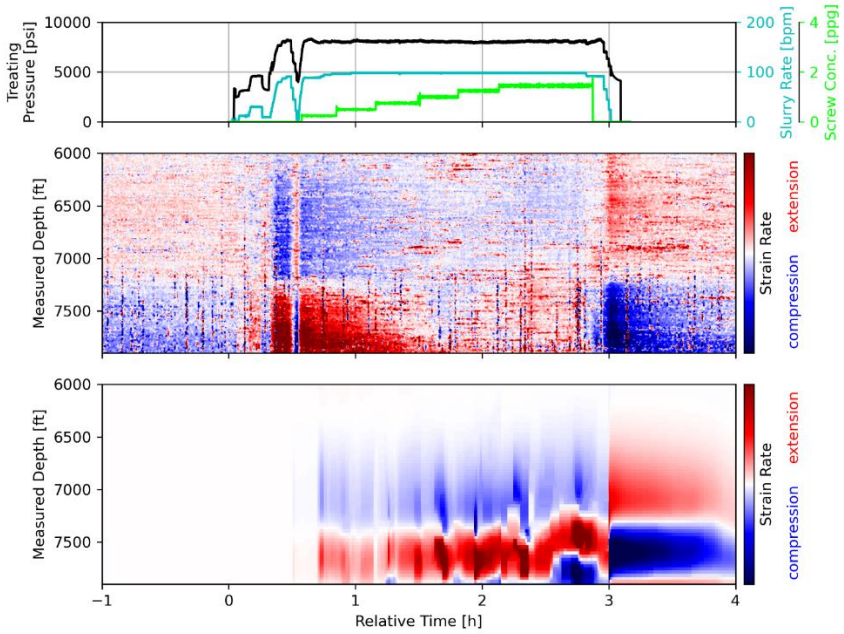

Figure 15: Treatment plot (top) and low-frequency distributed acoustic sensing (LF-DAS) cross-well strain response measured along Monitoring Well 73-22 (bottom), and modeled LF-DAS response (bottom) during a typical treatment stage. The LF-DAS is measured in units of strain rate and represents relative strain changes in the axial dimension of the wellbore (i.e., the fiber effectively measures vertical strain). Warm colors correspond to extensional strains and cool colors correspond to compressional strains. The location of the observed polarity flips (in this case, at approximately 7,250 ft MD) is related to the location of the upper crack tip of the fractures propagating away from the wellbore during the stimulation treatment (i.e., it is a measure of the fracture height).

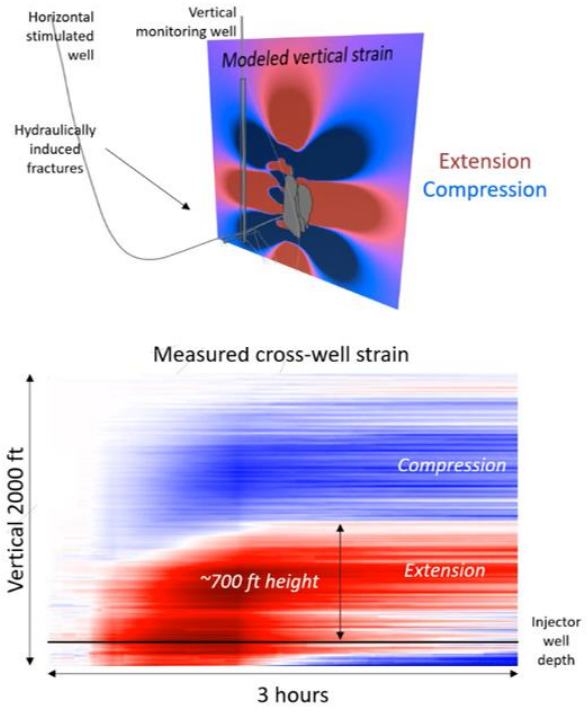

Figure 16: Reservoir simulation model result of the three-dimensional elastic strain field induced by fracture propagation from a multicluster stimulation treatment (top), and an example of measured LF-DAS data from Monitoring Well 73-22 during a typical treatment stage. The model strain field shows the vertical component of the strain tensor, which is consistent with the response that is measured by the fiber optic cable. The model indicates that the location of the polarity flip from compression to extension is strongly related to the vertical dimension of the propagating fractures.

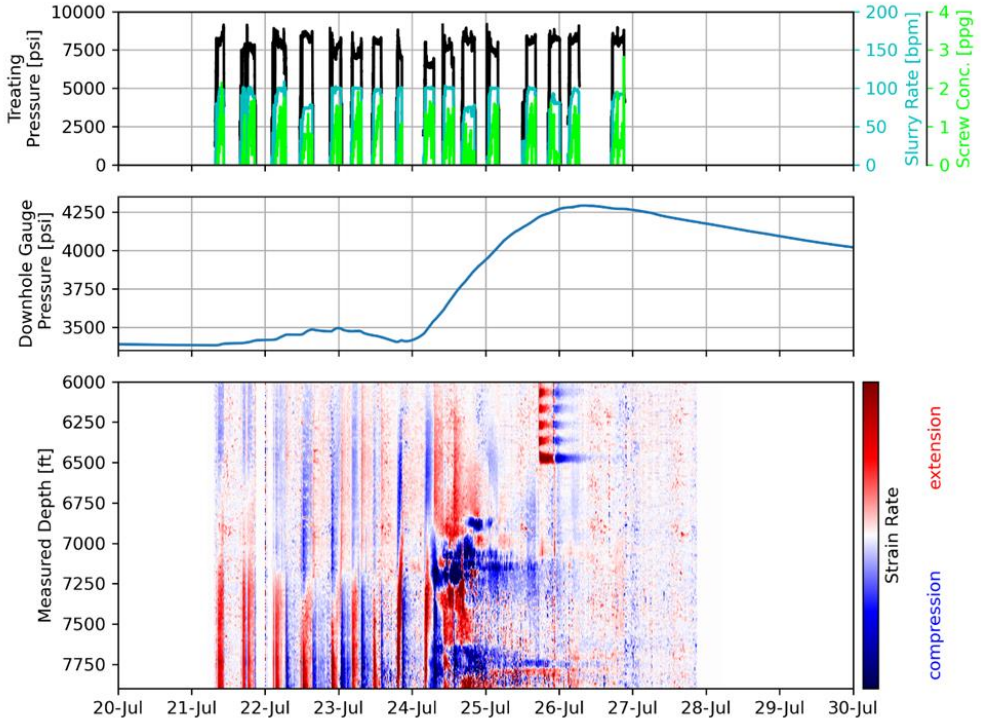

Figure 17: Treatment plots for all 16 stimulated stages (top); reservoir pressure recorded by a downhole gauge cemented behind casing at 7,720 ft in Monitoring Well 73-22 (middle); LF-DAS data recorded in 73-22.

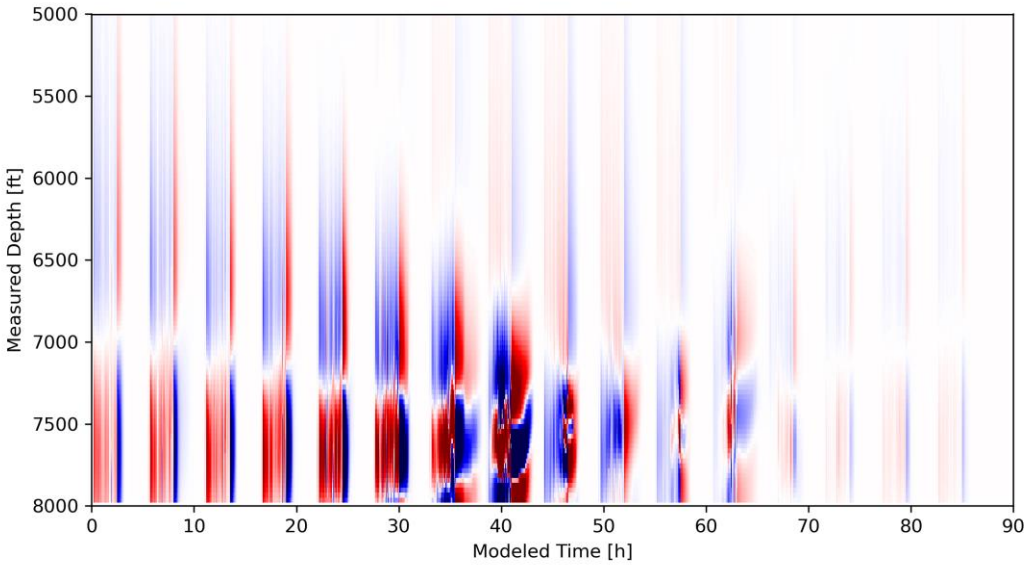

Figure 18: Modeled cross-well strain response from a 16-stage stimulation treatment. The modeled behavior closely replicates the measured LF-DAS response, including a broader process zone observed in early stages, a tighter process zone in stages that are closer to the monitoring well location, a more complex response for stages in the direct vicinity of the monitoring well location, and a markedly muted response for later stages. The lower response signal in the later stages can be explained by a geometrical effect related to the fracture propagation orientation.

6. CONCLUSIONS

Fervo Energy has designed and constructed a first-of-a-kind horizontal well geothermal development program. A horizontal doublet well system was drilled in the southern margin of the Blue Mountain geothermal field (Injection Well 34A-22 and Production Well 34-22), and a deep vertical monitoring well was also drilled for the purposes of reservoir characterization and stimulation treatment monitoring (Monitoring Well 73-22). The target reservoir lithology is a predominantly metasedimentary (phyllite and quartzite) with granitic intrusives (diorite and granodiorite). The laterals of the two horizontal wells were landed at a true vertical depth of approximately 7,700 ft and the productive lateral sections each extended roughly 3,250 ft. The curve sections were drilled at build rates of approximately 10 degrees of inclination per 100 ft from vertical up to fully horizontal (inclinations along the lateral range from 87° to 92°). The maximum recorded temperature along the lateral was 376 °F. While drilling, the downhole temperature was measured using an MWD tool near the bit, and we observed that downhole temperatures never exceeded 250 °F. The horizontal wells were drilled from the same pad. The optimal production well trajectory required successfully drilling a complex three-dimensional curve with a combination of back-build and lateral step-out. No wellbore stability issues were observed.

A 16-stage plug-and-perforate style stimulation treatment was performed on Injection Well 34A-22. A total of 17,000 bbl of slickwater fluid and 7.3 million lbs of proppant were pumped during the stimulation. In-well DAS measurements confirmed that fractures initiated at 100% of the perforation clusters, indicating that fracture breakdown and initiation is not a major barrier in hard rock lithologies. In-well DTS measurements were used to evaluate the downhole temperature conditions that the wireline tools (zonal isolation plugs and perforation charges) were exposed to. We observed that significant wellbore cooling occurred due to injecting at high rates during wireline pumpdown operations and during the stimulation of each stage, such that wellbore temperatures never exceeded 300 °F (most stages never exceeded 250 °F).

The distribution of microseismic events as well as direct strain measurements and bottomhole pressure measurements in an offset vertical well were used to constrain the geometry of the stimulated reservoir volume created during the 34A-22 treatment. Median fracture length and fracture height were estimated to be approximately 1800 ft and 750 ft, respectively, which is large enough for economic reservoir performance.

Having successfully completed the drilling, completion, and well construction phase of the project, we have demonstrated that currently no technical barriers exist to developing horizontal well geothermal drilling programs in high-temperature, hard rock settings. The project was completed using drilling and completions tools and technology that already commonly exist in the industry. A major focus of the project was on executing a comprehensive data acquisition program, which included diagnostic fracture injection tests, downhole microseismic monitoring, in-well and cross well distributed fiber optic sensing, and reservoir pressure monitoring with downhole gauges. The combination of multiple independent datasets provided detailed insight into the downhole conditions during the stimulation treatment as well as a well-characterized understanding of the stimulated reservoir volume geometry and other properties that impact reservoir performance of the doublet well system. Reservoir simulation forecasts and history matching were able to replicate key reservoir response observations, indicating that physics-based modeling can effectively be used to evaluate reservoir performance of horizontal well geothermal systems.

ACKNOWLEDGMENTS

Funding provided by DOE EERE Geothermal Technologies Office to Utah FORGE and the University of Utah under Project DE-EE0007080 Enhanced Geothermal System Concept Testing and Development at the Milford City, Utah Frontier Observatory for Research in Geothermal Energy (Utah FORGE) site. Funding was also provided by DOE EERE Geothermal Technologies Office under Project DE-EE0008486.

REFERENCES

Faulds, N.H. and Hinz, N.H.: Favorable tectonic and structural settings of geothermal settings in the Great Basin Region, western USA: Proxies for discovering blind geothermal systems, Proceedings, World Geothermal Congress, Melbourne, Australia, (2016).

Fercho, S., Norbeck, J.H., McConville, E., et al.: Geology, state of stress, and heat in place for a horizontal well geothermal development project at Blue Mountain, Nevada, Proceedings, 48th Workshop on Geothermal Reservoir Engineering, Stanford University, Stanford, CA, (2023).

Gradl, C.: Review of recent unconventional completion innovations and their applicability to EGS wells, Proceedings, 43rd Workshop on Geothermal Reservoir Engineering, Stanford University, Stanford, CA, (2018).

Jin, G. and Roy, B.: Hydraulic-fracture geometry characterization using low-frequency DAS signal, The Leading Edge, 36(12), (2017), 975-980.

Latimer, T. and Meier, P.: Use of the experience curve to understand economics for at-scale EGS projects, Proceedings, 42nd Workshop on Geothermal Reservoir Engineering, Stanford University, Stanford, CA, (2017).

McClure, M.W. and Horne, R.N.: An investigation of stimulation mechanisms in Enhanced Geothermal Systems, Int. Journal of Rock Mechanics and Mining Sciences, 72, (2014), 242-260.

McClure, M.W., Jung, H., Cramer, D.D., and Sharma, M.M.: The fracture-compliance method for picking closure pressure from diagnostic fracture injection tests, SPE Journal, 21 (04), (2016), 1321-1339.

McClure, M.W., Kang, C., Hewson, C., et al.: ResFrac Technical Writeup, Technical report, ResFrac Corporation, (2022).

Norbeck, J.H., McClure, M.W., and Horne, R.N.: Field observations at the Fenton Hill enhanced geothermal system test site support mixed-mechanism stimulation, Geothermics, 74, (2018), 135-149.

Norbeck, J.H., McClure, M.W., Lo, J.W., and Horne, R.N.: An embedded fracture modeling framework for simulation of hydraulic fracturing and shear stimulation, Computational Geosciences, 20 (1), (2016), 1-18.

Ricks, W, Norbeck, J., Jenkins, J.: The value of in-reservoir energy storage for flexible dispatch of geothermal power, Applied Energy, 313, (2022), 118807.

Sepulveda, N., Jenkins, J., de Sisternes, F., and Lester, R.: The role of firm low-carbon electricity resources in deep decarbonization of power generation, Joule, 2(11), (2018), 2403–20, http://dx.doi.org/10.1016/j.joule.2018.08.006.

Sherman, C., Mellors, R., Morris, J., and Ryerson, F.: Geomechanical modeling of distributed fiber-optic sensor measurements, Interpretation, 7(1), (2019), SA21-SA27.

Somanchi, K., Brewer, J., and Reynolds, A.: Extreme limited-entry design improves distribution efficiency in plug-and-perforate completions: Insights from fiber-optic diagnostics, SPE Drilling and Completions, 33(04), (2018), 298-306.

Shiozawa, S. and McClure, M.W.: EGS designs with horizontal wells, multiple stages, and proppant, Proceedings, 39th Workshop on Geothermal Reservoir Engineering, Stanford University, Stanford, CA, (2014).

Szybinski, Z.A.: Structural Setting of the Blue Mountain Geothermal Project Area, Humboldt County, Nevada, unpublished report for Nevada Geothermal Power Inc, (2005).

Weijers, L., Wright, C., Mayerhofer, M., Pearson, M., Griffin, L., Weddle, P.: Trends in the North American frac industry: Invention through shale revolution, Paper SPE 194345-MS, SPE Hydraulic Fracturing Technology Conference and Exhibition, The Woodlands, Texas, USA, (2019).

APPENDIX

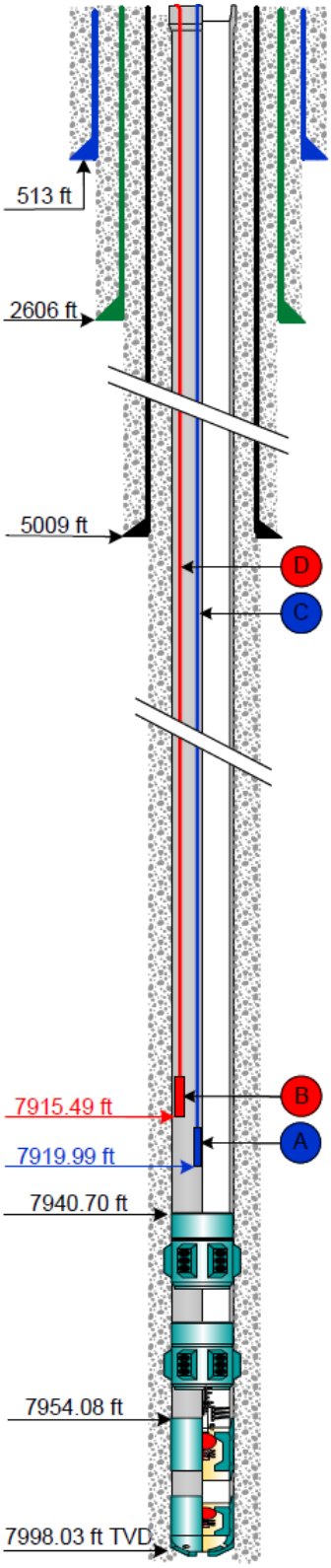

Fervo BM 73-22 Monitoring Well

Final Installation Report

Company	Fervo Energy	API No.	27-013-90148
Prepared for	Jack Norbeck	Phone	Location: Humboldt County, Nevada BM 73-22
Prepared by	Mark Woitt	Phone	
Service center		Phone	Date: 1/24/2023 Page: 1

Tubular	Size (in.)	Weight (lbs/ft)	Grade	Thread	Hole Size (in)	Bottom Depth (ft.KB)
Surface Casing	20	106	K-55		24	513
Intermediate Casing	13.375	68	K-55		17.5	2606
Intermediate Casing	9.625	36	K-55		12.25	5009
Production Casing	4.50	11.6	P-110		8.75	7998.03

ITEM	Instrumentation Equipment Description	ID	OD	Length (ft)	Depth (ft)
A.	Permanent Pressure/ Temperature Sensor				7919.99
B.	Fiber Optic Termination Sub				7915.49
C.	Tubing Encapsulated Instrument Cable			7919.99	
D.	Fiber Optic Cable, 2 X Multi-Mode and 2 X Single-Mode			7915.49	

REMARKS

Figure A1: Well construction diagram for Monitoring Well 73-22.

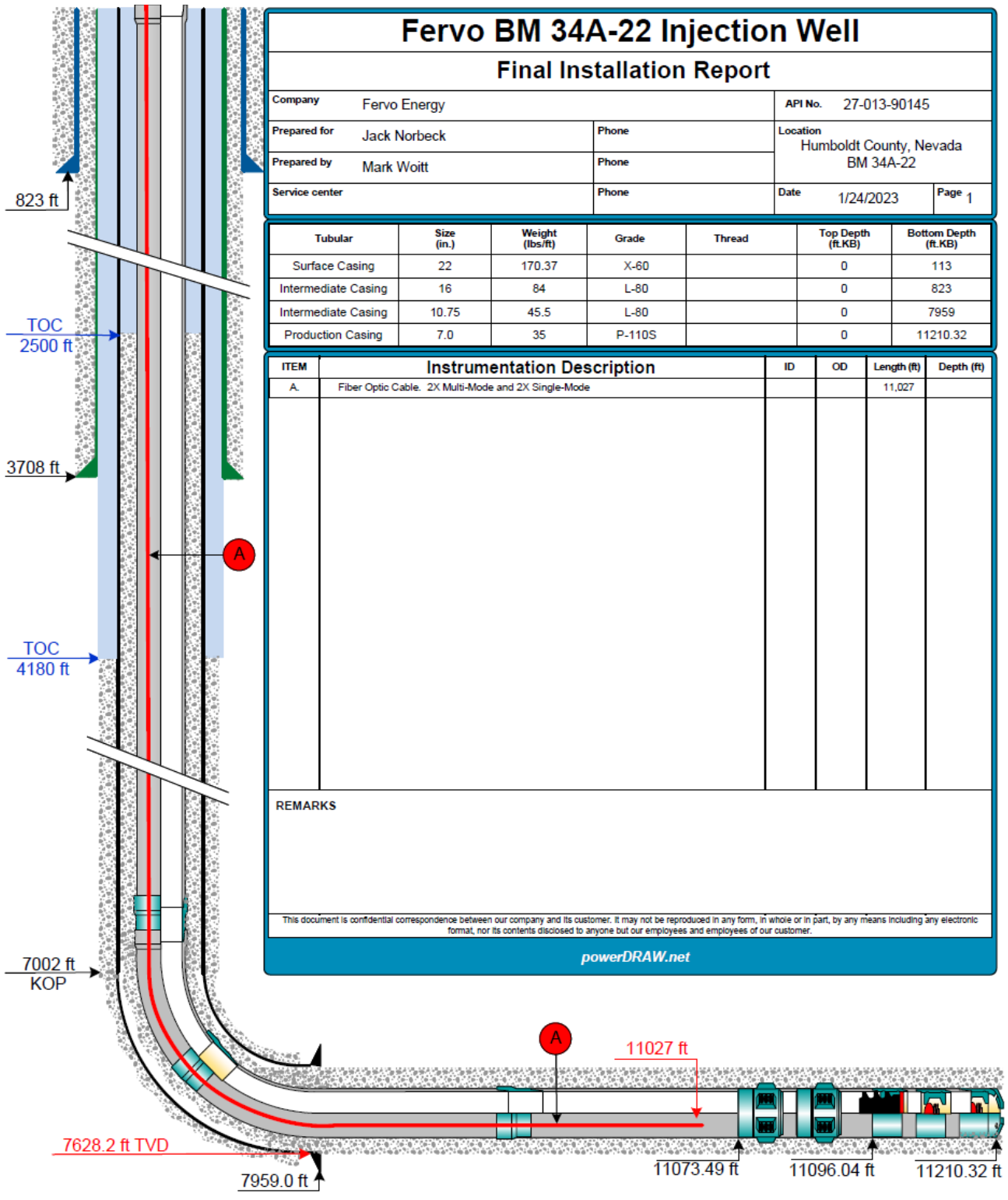

Fervo BM 34A-22 Injection Well

Final Installation Report

Company	Fervo Energy	API No.	27-013-90145
Prepared for	Jack Norbeck	Phone	Location: Humboldt County, Nevada BM 34A-22
Prepared by	Mark Woitt	Phone	
Service center		Phone	Date: 1/24/2023 Page: 1

Tubular	Size (in.)	Weight (lbs/ft)	Grade	Thread	Top Depth (ft.KB)	Bottom Depth (ft.KB)
Surface Casing	22	170.37	X-60		0	113
Intermediate Casing	16	84	L-80		0	823
Intermediate Casing	10.75	45.5	L-80		0	7959
Production Casing	7.0	35	P-110S		0	11210.32

ITEM	Instrumentation Description	ID	OD	Length (ft)	Depth (ft)
A.	Fiber Optic Cable. 2X Multi-Mode and 2X Single-Mode			11,027	

REMARKS

Figure A2: Well construction diagram for Injection Well 34A-22.

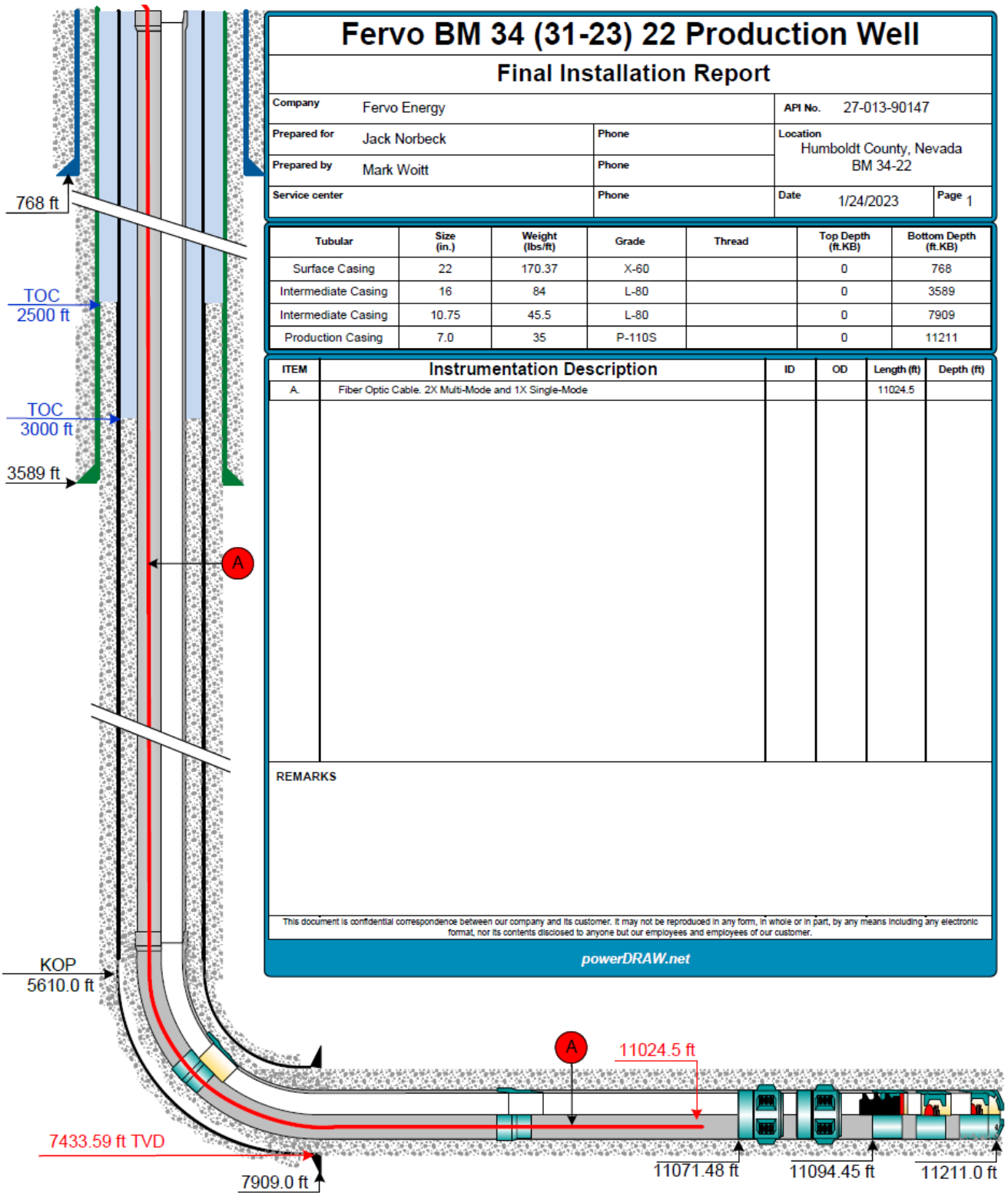

Fervo BM 34 (31-23) 22 Production Well

Final Installation Report

Company	Fervo Energy	API No.	27-013-90147
Prepared for	Jack Norbeck	Phone	Location: Humboldt County, Nevada BM 34-22
Prepared by	Mark Woitt	Phone	
Service center		Phone	Date: 1/24/2023 Page 1

Tubular	Size (in.)	Weight (lbs/ft)	Grade	Thread	Top Depth (ft.KB)	Bottom Depth (ft.KB)
Surface Casing	22	170.37	X-60		0	768
Intermediate Casing	16	84	L-80		0	3589
Intermediate Casing	10.75	45.5	L-80		0	7909
Production Casing	7.0	35	P-110S		0	11211

ITEM	Instrumentation Description	ID	OD	Length (ft)	Depth (ft)
A.	Fiber Optic Cable. 2X Multi-Mode and 1X Single-Mode			11024.5	

REMARKS

Figure A3: Well construction diagram for Production Well 34-22.

Table A1. Bit record for Monitoring Well 73-22.

No.	Bit Size (in)	Type	Footage Drilled (ft)	Bit Life (hours)	Avg ROP (ft/hr)	Avg On-Bottom ROP (ft/hr)	Max ROP (ft/hr)
1	26	Milltooth Bit	411	32	13	30	31
2	17.5	Insert Bit	434	18	24	36	42
3	17.5	Insert Bit	154	13	12	17	31
4	17.5	Insert Bit	1496	58	26	35	42
5	12.25	Hybrid Bit	391	9	43	46	52
6	12.25	Hybrid Bit	2012	59	34	46	55
7	8.75	Mill tooth Bit	5	0	20	45	65
8	8.75	Hybrid Bit	78	2	36	44	51
9	8.75	Hybrid Bit	1081	36	30	39	52
10	8.75	PDC Bit	831	35	24	32	49
11	8.75	PDC Bit	1000	58	17	22	42

Table A2. Bit record for Injection Well 34A-22.

No.	Bit Size (in)	Type	Footage Drilled (ft)	Bit Life (hours)	Avg ROP (ft/hr)	Avg On-Bottom ROP (ft/hr)	Max ROP (ft/hr)
1	26	Milltooth Bit	714	43	17	25	42
2	20	Rock Bit	2473	51	49	63	77
3	20	Rock Bit	413	17	24	36	63
4	14.75	PDC Bit	934	39	24	39	70
5	14.75	Insert Bit	380	19	20	28	44
6	14.75	PDC Bit	145	37	4	12	23
7	14.75	PDC Bit	1283	40	32	50	82
8	14.75	PDC Bit	507	NA	NA	21	34
9	14.75	Hybrid	1004	73	14	18	29
10	14.75	Hybrid	190	22	9	12	22
11	14.75	Insert Bit	463	44	10	13	23
12	9.875	PDC Bit	725	44	17	25	48
13	9.875	PDC Bit	187	11	18	24	34
14	9.875	Insert Bit	499	60	8	11	19
15	9.875	Hybrid Bit	356	31	11	20	41
16	9.875	PDC Bit	438	48	9	15	31
17	9.875	Insert Bit	274	41	7	9	16
18	9.875	Insert Bit	352	42	9	11	20
19	9.875	PDC Bit	420	29	15	22	41

Table A3. Bit record for Production Well 34-22.

No.	Bit Size (in)	Type	Footage Drilled (ft)	Bit Life (hours)	Avg ROP (ft/hr)	Avg On-Bottom ROP (ft/hr)	Max ROP (ft/hr)
1	26	Milltooth Bit	676	32	21	28	33
2	20	Insert Bit	2827	81	35	50	74
3	14.75	Insert Bit	1907	82	23	28	43
4	14.75	Insert Bit	1510	79	19	25	36
5	14.75	Hybrid Bit	157	12	13	18	31
6	14.75	Insert Bit	731	55	13	17	28
7	9.875	Insert Bit	395	30	13	20	32
8	9.875	Insert Bit	65	12	6	7	10
9	9.875	Insert Bit	361	29	13	27	48
10	9.875	Insert Bit	3	7	0	1	2
11	9.875	Insert Bit	173	14	13	15	24
12	9.875	Insert Bit	648	51	13	17	26
13	9.875	Insert Bit	280	19	15	19	29
14	9.875	Insert Bit	560	52	11	12	21
15	9.875	PDC Bit	825	36	23	33	56